Effect of Shockley-Read-Hall recombination on the static and dynamical characteristics of epitaxial quantum-dot lasers on silicon

Shiyuan Zhao ⬥*

LTCI, Télécom Paris, Institut Polytechnique de Paris, 19 place Marguerite Perey, 91120 Palaiseau, France

Frédéric Grillot

LTCI, Télécom Paris, Institut Polytechnique de Paris, 19 place Marguerite Perey, 91120 Palaiseau, France
and Center for High Technology Materials, University of New Mexico, Albuquerque, New Mexico 87106, USA

We semianalytically and numerically investigate the static and dynamical characteristics of quantum-dot (QD) lasers directly grown on silicon by considering the Shockley-Read-Hall (SRH) recombination. The static characteristics are studied through small-signal analysis, including the α_H factor, damping factor, and modulation dynamics. In addition, the feedback dynamics are analyzed through improved corpuscular rate equations based on the classical Lang-Kobayashi (LK) model with time series, bifurcation diagrams, and phase portraits. We find that a smaller α_H factor but larger damping factor are obtained by decreasing the nonradiative recombination lifetime. On top of that, in both the short- and long-external-cavity regimes, any decrease of the SRH recombination lifetime obliterates significantly chaotic regions and shifts the first Hopf bifurcation point to higher feedback values. Overall, this work provides insights into the understanding of QD laser physics, hence highlighting the influence of the SRH lifetime on the reflection sensitivity of epitaxial QD lasers on silicon. These results are qualitatively consistent with recent experiments and are therefore helpful for designing feedback-resistant lasers for future photonic integrated circuits operating without optical isolation.

I. INTRODUCTION

Silicon photonics is considered a mainstream data-transmission solution for next-generation data centers and is progressing rapidly to enable photonic integrated circuits (PICs) with a very small footprint and substantial energy efficiency [1,2]. In this context, the direct growth of III-V semiconductor materials on silicon has nowadays become one of the most pressing concerns in the semiconductor laser field [3]. Owing to the full quantization of electrons and holes and the reduced sensitivity to crystalline defects, quantum-dot (QD) lasers directly grown on silicon are envisioned as powerful candidates for integrated silicon technologies, hence exhibiting remarkable properties, including, but not limited to, low threshold current, high-temperature stability, and robust tolerance to external optical feedback (EOF) [4]. This latter property is of utmost importance for achieving large-scale integrated circuits in which unintentional back-reflections produced by the various passive and active interfaces can strongly hinder the stability of the lasers. This effect is, indeed, highly detrimental in PICs because light emitters are tightly assembled with other optical components (e.g., modulators, waveguides, etc.) to achieve the desired functionality, hence resulting in possible optical reflections on the silicon integrated devices. To overcome this problem, an optical isolator is inserted to block the feedback light in the active

region and to avoid potential laser instabilities but at the price of a much higher cost. Therefore, the development of feedback-insensitive lasers remains a major objective for silicon photonic integration. In this view, it is known that QD lasers are more resistant to EOF than their bulk or quantum-well (QW) counterparts, which essentially results from the smaller α_H factor [5] and the larger damping [6]. In some cases, the large contrast ratio of the excited-to-ground-state lasing thresholds was also found to be highly beneficial for maintaining a high degree of stability [7].

Nevertheless, over the past few years, the crystal-lattice mismatch between the silicon and III-V laser materials has been a crucial problem that has strongly limited the development of direct integration of laser sources on silicon-based PICs. Indeed, the mismatch in the lattice constant and thermal expansion coefficients causes the generation of threading dislocation (TD), which acts as nonradiative recombination centers through the Shockley-Read-Hall (SRH) process, hence leading to deleterious effects on the device performance [8]. Although tremendous efforts have been devoted to improving the quality of QD lasers directly grown on silicon, the achievable TD density is still around 10^5–10^6 cm^{-2}. The aim of this work is to theoretically investigate the static characteristics and reflection-sensitivity problem of QD lasers directly grown on silicon by studying the peculiar role of the epitaxial defects. To do so, we numerically analyze such properties with the help of the improved rate-equation model taking into account the nonradiative recombination due to the SRH process.
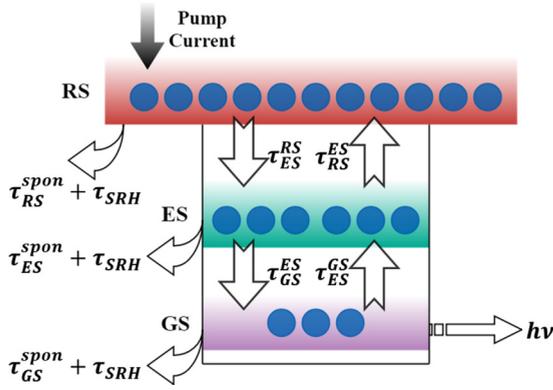
*shiyuan.zhao@telecom-paris.fr

FIG. 1. Schematic representation of the electronic structure and carrier dynamics of QD lasers on silicon. The ES transition energy is 0.87 eV, and its energy separation is 0.1 eV with the RS and 0.05 eV with the GS.

This paper is organized as follows: Section II introduces the modeling framework as well as the relationship between the TD density and SRH recombination lifetime. In particular, the SRH lifetime τ_{SRH} is incorporated into the corpuscular rate-equation system. Section III investigates the static characteristics through the small-signal analysis of QD laser system by considering the α_H factor and modulation dynamics. Section IV investigates nonlinear laser dynamics subject to the EOF in both short- and long-cavity regimes. The dynamics are fully analyzed with time series, bifurcation diagrams, and phase portraits. In particular the simulations focus on the first Hopf bifurcation, which is known to play a crucial role in the route to chaos via period-doubling regimes or quasiperiodicity. The results show that the laser destabilization which takes place at the first Hopf bifurcation associated with the undamping of the laser's relaxation oscillations is linked to the value of the SRH recombination lifetime. Finally, Sec. V summarizes the results and provides conclusions on the work conducted. Overall, we believe that these results can be useful for designing novel feedback-resistant lasers for future PICs operating without optical isolator.

II. MODELING FRAMEWORK

The QD laser electronic structure can be simplified as the three-level rate-equation model [9], which consists of the two-dimensional carrier reservoir state (RS) and the QD ensemble within the active region, including two energy levels: the off-resonant fourfold-degenerate excited states (ESs) and the resonant twofold-degenerate ground state (GS). For the sake of brevity, the laser is assumed to have only one QD ensemble, and electrons and holes are considered to be neutral excitons. Its schematic representation is depicted in Fig. 1; the external carriers are originally diffused into the RS from the contact, and then some of them are captured in the ES within lifetime τ_{ES}^{RS} or are recombined spontaneously within the spontaneous emission time $\tau_{RS}^{\mathrm{spon}}$. On the contrary, carriers can be thermally relaxed from the ES to the RS within escape time τ_{RS}^{ES}, which is governed by the Fermi distribution for the quasiequilibrium without external excitation. Similar carrier behavior is presented for the carrier population between the ES and GS in

the dots. It is necessary to point out that this work proposes an improved rate-equation model by taking into account the effect of the SRH recombination within lifetime τ_{SRH} in each level. Thus, the corpuscular rate equations describing carrier population $N_{RS,ES,GS}$ and complex electric-field dynamics are expressed as

$$\frac{dN_{RS}}{dt} = \frac{\eta I}{q} + \frac{N_{ES}}{\tau_{RS}^{ES}} - \frac{N_{RS}}{\tau_{ES}^{RS}}(1 - \rho_{ES})$$
$$- \frac{N_{RS}}{\tau_{RS}^{\mathrm{spon}}} - \frac{N_{RS}}{\tau_{SRH}} + F_{RS}, \tag{1}$$

$$\frac{dN_{ES}}{dt} = \left(\frac{N_{RS}}{\tau_{ES}^{RS}} + \frac{N_{GS}}{\tau_{ES}^{GS}}\right)(1 - \rho_{ES}) - \frac{N_{ES}}{\tau_{RS}^{ES}}$$
$$- \frac{N_{ES}}{\tau_{GS}^{ES}}(1 - \rho_{GS}) - \frac{N_{ES}}{\tau_{ES}^{\mathrm{spon}}} - \frac{N_{ES}}{\tau_{SRH}} + F_{ES}, \tag{2}$$

$$\frac{dN_{GS}}{dt} = \frac{N_{ES}}{\tau_{GS}^{ES}}(1 - \rho_{GS}) - \frac{N_{GS}}{\tau_{ES}^{GS}}(1 - \rho_{ES})$$
$$- \Gamma_p v_g g_{GS}|E_{GS}|^2 - \frac{N_{GS}}{\tau_{GS}^{\mathrm{spon}}} - \frac{N_{GS}}{\tau_{SRH}} + F_{GS}, \tag{3}$$

$$\frac{dE_{GS}}{dt} = \frac{1}{2}\left(\Gamma_p v_g g_{GS} - \frac{1}{\tau_p}\right)E_{GS} + \frac{j}{2}\Gamma_p v_g$$
$$\times \left(g_{GS}\alpha_H^{GS} + g_{ES}\alpha_H^{ES} + g_{RS}\alpha_H^{RS}\right)E_{GS} + F_E, \tag{4}$$

with I being the pump bias current, q being the electron charge, η being the pump efficiency, Γ_p being the optical confinement factor, v_g being the group velocity, τ_p being the photon lifetime, and $F_{RS,ES,GS,E}$ being the Langevin noise terms. It is worth mentioning that only the stimulated emission originating from the GS level is considered; hence, E_{GS} accounts for the complex electric field in the GS level. The gain $g_{RS,ES,GS}$ of each state is expressed by introducing the differential gain $a_{RS,ES,GS}$:

$$g_{GS} = \frac{a_{GS}}{1 + \varepsilon|E_{GS}|^2}\frac{N_B}{V_B}(2\rho_{GS} - 1), \tag{5}$$

$$g_{ES} = a_{ES}\frac{N_B}{V_B}(2\rho_{ES} - 1), \tag{6}$$

$$g_{RS} = a_{RS}\frac{D_{RS}}{V_{RS}}(2\rho_{ES} - 1), \tag{7}$$

where ε is the gain compression factor, N_B is the total number of QDs, V_B is the volume of the active region, D_{RS} is the total number of states in the RS, V_{RS} is the volume of the RS, and $\rho_{GS,ES,RS}$ are the occupation probabilities in the GS, ES, and RS, which are given by $\rho_{GS} = \frac{N_{GS}}{2N_B}$, $\rho_{ES} = \frac{N_{ES}}{4N_B}$, and $\rho_{RS} = \frac{N_{RS}}{D_{RS}}$, respectively. In Eqs. (4), α_H^{GS} is the GS contribution to the α_H factor, and $\alpha_H^{ES,RS}$ are defined by

$$\alpha_H^{ES,RS} = \frac{\omega_{GS}}{\omega_{ES,RS}}\frac{(\omega_{ES,RS} - \omega_{GS})T_D}{1 + (\omega_{ES,RS} - \omega_{GS})^2 T_D^2}, \tag{8}$$

with T_D being the dephasing time. Furthermore, the dynamics of a single-mode semiconductor laser under external optical feedback is described by the classical Lang-Kobayashi (LK) rate equations using delay differential equations [10]. The

LK system has been explored for more than 20 years now by means of extensive analytical and experimental studies [11,12]. A number of textbooks have been published that are of great interest [13]. Thanks to this approach, we can incorporate feedback terms into our model. Meanwhile, through the relationship $E_{GS}(t) = \sqrt{S_{GS}(t)/\Gamma_p} e^{j\phi(t)}$, the photon number S_{GS} and the phase ϕ are separately described as

$$\frac{dS_{GS}}{dt} = \left(\Gamma_p v_g g_{GS} - \frac{1}{\tau_p}\right)S_{GS} + \beta_{sp}\frac{N_{GS}}{\tau_{GS}^{\text{spon}}}$$
$$+ \frac{k_c}{\tau_{\text{in}}}\sqrt{S_{GS}(t-\tau)S_{GS}(t)}\cos(\Delta) + F_S, \qquad (9)$$

$$\frac{d\phi}{dt} = \frac{1}{2}\Gamma_p v_g \left(g_{GS}\alpha_H^{GS} + g_{ES}\alpha_H^{ES} + g_{RS}\alpha_H^{RS}\right)$$
$$- \frac{k_c}{\tau_{\text{in}}}\sqrt{\frac{S_{GS}(t-\tau)}{S_{GS}(t)}}\sin(\Delta) + F_\phi, \qquad (10)$$

with β_{sp} being the spontaneous emission factor, τ_{in} being the internal cavity photon round-trip time, and τ being the external cavity photon round-trip time. Parameter k_c is the optical feedback term written as $k_c = \frac{1-R}{\sqrt{R}}f_{\text{ext}}$, where $R = 0.32$ is the mirror reflectivity and f_{ext} is the feedback strength. Δ is defined as $\Delta = \psi_0 + \phi(t) - \phi(t-\tau)$ according to the LK model, where ψ_0 is the initial phase shift.

As already stated, the direct growth of QDs on a silicon substrate is associated with several challenges like limiting the epitaxial defects because those lead to multiple nonradiative recombination centers through the SRH process. The relation between the nonradiative recombination lifetime and the defect density can be written as follows [14]:

$$\frac{1}{\tau_{SRH}} = \frac{1}{\tau_{SRH}^0} + \frac{D\pi^3\sigma}{4}, \qquad (11)$$

with $\tau_{SRH}^0 = 1877$ ns being the lifetime of dislocation-free GaAs-based QD lasers, $D = 10$ cm^2 s^{-1} being the average diffusion coefficient, and σ being the TD density value. The epitaxial defect density in QD lasers on native substrate is typically in the range of 10^3–10^4 cm^{-2} or even less, and consequently, the corresponding τ_{SRH} is on the order of 10 ns,
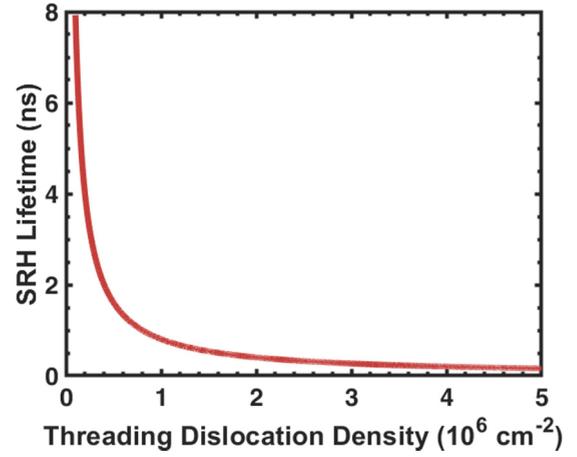

FIG. 2. Calculated SRH recombination lifetime obtained with an approximation method [14] as a function of TD density.

which is much longer than the spontaneous emission lifetime (~ 1.0 ns). Therefore, for such QD lasers, this additional nonradiative recombination term can be fully neglected in our model without loss of generality. Nevertheless, a different situation occurs in Si-based QD lasers where the defect density (10^6–10^8 cm^{-2}) is at least two orders of magnitude higher than that in GaAs-based QD ones [15]. Here, the nonradiative carrier lifetime can be as low as 0.1 ns, which becomes shorter than the spontaneous emission lifetime, as shown in Fig. 2.

In what follows, the peculiar effect of the SRH recombination on the QD laser's static and dynamical features is analyzed through the numerical simulations.

III. EFFECT OF SHOCKLEY-READ-HALL RECOMBINATION ON THE STATIC PERFORMANCE

In this section, the QD laser static characteristics are investigated via a small-signal analysis. Assuming a sinusoidal current modulation $\delta I = I_0 e^{j\omega t}$ with modulation frequency ω, this change will induce the variations of carriers $\delta N_{RS,ES,GS}$, photon number δS_{GS}, and phase $\delta\phi$. Therefore, the corresponding matrix can be derived as

$$\begin{bmatrix} \gamma_{11} + j\omega & -\gamma_{12} & 0 & 0 & 0 \\ -\gamma_{21} & \gamma_{22} + j\omega & -\gamma_{23} & 0 & 0 \\ 0 & -\gamma_{32} & \gamma_{33} + j\omega & -\gamma_{34} & 0 \\ 0 & 0 & -\gamma_{43} & \gamma_{44} + j\omega & 0 \\ -\gamma_{51} & -\gamma_{52} & -\gamma_{53} & -\gamma_{54} & j\omega \end{bmatrix}\begin{bmatrix} \delta N_{RS} \\ \delta N_{ES} \\ \delta N_{GS} \\ \delta S_{GS} \\ \delta\phi \end{bmatrix} = \frac{\eta I}{q}\begin{bmatrix} 1 \\ 0 \\ 0 \\ 0 \\ 0 \end{bmatrix}, \qquad (12)$$

with

$$\gamma_{11} = \frac{1 - \rho_{ES}}{\tau_{ES}^{RS}} + \frac{1}{\tau_{RS}^{\text{spon}}} + \frac{1}{\tau_{SRH}},$$

$$\gamma_{12} = \frac{1}{\tau_{RS}^{ES}} + \frac{1}{4N_B}\frac{N_{RS}}{\tau_{ES}^{RS}}, \quad \gamma_{21} = \frac{1 - \rho_{ES}}{\tau_{ES}^{RS}},$$

$$\gamma_{22} = \frac{1 - \rho_{GS}}{\tau_{GS}^{ES}} + \frac{1}{\tau_{RS}^{ES}} + \frac{1}{\tau_{ES}^{\text{spon}}} + \frac{1}{4N_B}\left(\frac{N_{RS}}{\tau_{ES}^{RS}} + \frac{N_{GS}}{\tau_{ES}^{GS}}\right) + \frac{1}{\tau_{SRH}},$$

$$\gamma_{23} = \frac{1 - \rho_{ES}}{\tau_{ES}^{GS}} + \frac{1}{2N_B}\frac{N_{ES}}{\tau_{GS}^{ES}}, \quad \gamma_{32} = \frac{1 - \rho_{GS}}{\tau_{GS}^{ES}} + \frac{1}{4N_B}\frac{N_{GS}}{\tau_{ES}^{GS}},$$

$$\gamma_{33} = \frac{1 - \rho_{ES}}{\tau_{ES}^{GS}} + \frac{1}{2N_B} \frac{N_{ES}}{\tau_{GS}^{ES}} + \frac{1}{\tau_{GS}^{\text{spon}}} + \frac{1}{\tau_{SRH}} + \Gamma_p v_g a S_{GS},$$

$$\gamma_{34} = -\Gamma_p v_g g_{GS} + \Gamma_p v_g a_p S_{GS},$$

$$\gamma_{43} = \Gamma_p v_g a S_{GS} + \frac{\beta_{sp}}{\tau_{GS}^{\text{spon}}}, \quad \gamma_{44} = \frac{1}{\tau_p} - \Gamma_p v_g g_{GS} + \Gamma_p v_g a_p S_{GS},$$

$$\gamma_{51} = \Gamma_p v_g a_{RS} \alpha_H^{RS}, \quad \gamma_{52} = \frac{1}{4} \Gamma_p v_g a_{ES} \alpha_H^{ES},$$

$$\gamma_{53} = \frac{1}{2} \Gamma_p v_g a \alpha_H^{GS}, \quad \gamma_{54} = -\frac{1}{2} \Gamma_p v_g a_p \alpha_H^{GS},$$

where a and a_p take into account the gain compression at high photon number such as $dg_{GS} = adN_{GS} - a_p dS_{GS}$:

$$a = \frac{\partial g_{GS}}{\partial N_{GS}} = \frac{a_{GS}}{1 + \varepsilon S_{GS}}, \quad a_p = -\frac{\partial g_{GS}}{\partial S_{GS}} = \frac{\varepsilon g_{GS}}{1 + \varepsilon S_{GS}}.$$

Based on this method, the laser's static properties are investigated in the following sections. The most relevant material and optical parameters used in our simulations for the QD laser are given in Table I if not otherwise specified. And the photon number is fixed during our simulations at 2×10^5.

A. Impact on the α_H factor

Considering the above differential rate equations, the modulation-frequency-dependent α_H factor of the QD laser is

TABLE I. Material and optical parameters of the QD laser used in the simulation.

Symbol	Description	Value
E_{RS}	RS energy level	0.97 eV
E_{ES}	ES energy level	0.87 eV
E_{GS}	GS energy level	0.82 eV
τ_{ES}^{RS}	RS to ES capture time	6.3 ps
τ_{GS}^{ES}	ES to GS relaxation time	2.9 ps
τ_{RS}^{ES}	ES to RS escape time	2.7 ns
τ_{ES}^{GS}	GS to ES escape time	10.4 ps
τ_{RS}^{spon}	RS spontaneous emission lifetime	0.5 ns
τ_{ES}^{spon}	ES spontaneous emission lifetime	0.5 ns
τ_{GS}^{spon}	GS spontaneous emission lifetime	1.2 ns
τ_p	Photon lifetime	4.1 ps
T_D	Polarization dephasing time	0.1 ps
τ_{SRH}	Nonradiative recombination lifetime	0.1–10 ns (variable)
β_{sp}	Spontaneous emission factor	1×10^{-4}
ε	Gain compression factor	2×10^{-16} cm^3
Γ_p	Optical confinement factor	0.06
a_{GS}	GS differential gain	5×10^{-15} cm^2
a_{ES}	ES differential gain	10×10^{-15} cm^2
a_{RS}	RS differential gain	2.5×10^{-15} cm^2
α_H^{GS}	GS contribution to α_H factor	0.5
N_B	Total QD number	1×10^7
D_{RS}	Total RS state number	4.8×10^6
V_B	The volume of active region	5×10^{-11} cm^3
V_{RS}	The volume of RS region	1×10^{-11} cm^3

derived as follows [16]:

$$\alpha_H(\omega) = \frac{2}{\Gamma_p v_g} \frac{\left[\Delta \omega_N^{\text{Total}}(N)\right]}{\delta g_{GS}(N)}$$

$$= \alpha_H^{GS} + \frac{1}{2} \alpha_H^{ES} \frac{a_{ES} \delta N_{ES}}{a \delta N_{GS}} + 2\alpha_H^{RS} \frac{a_{RS} \delta N_{RS}}{a \delta N_{GS}}. \quad (13)$$

It should be emphasized that only the carrier contribution δN is included in the above equation, while the photon contribution δS is excluded. Actually, the ratios $\frac{\delta N_{RS}}{\delta N_{GS}}$ and $\frac{\delta N_{ES}}{\delta N_{GS}}$ include implicitly τ_{SRH} if we use Cramer's rule in Eqs. (12) considering only three carrier equations:

$$\frac{\delta N_{RS}}{\delta N_{GS}} = \frac{\gamma_{12} \gamma_{23}}{(\gamma_{11} + j\omega)(\gamma_{22} + j\omega) - \gamma_{12} \gamma_{21}},$$

$$\frac{\delta N_{ES}}{\delta N_{GS}} = \frac{-\gamma_{11} \gamma_{23}}{(\gamma_{11} + j\omega)(\gamma_{22} + j\omega) - \gamma_{12} \gamma_{21}}.$$

As shown in Fig. 3, the α_H factor of QD lasers using Eqs. (13) is, indeed, dependent on the modulation frequency. Such a difference is due to the carrier density variations in the three states (e.g., GS, ES, and RS) that significantly impact the α_H factor under direct modulation. Thus, for low
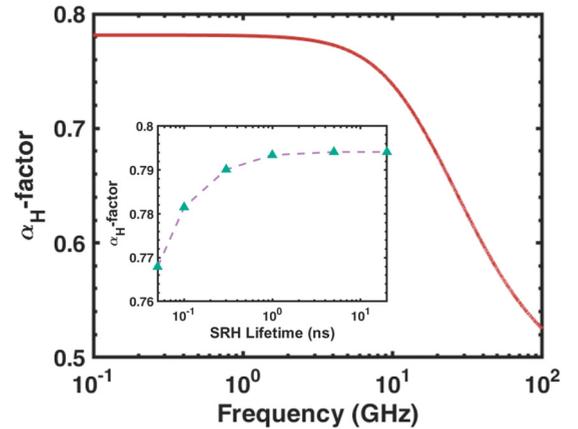

FIG. 3. The modulation-frequency-dependent α_H factor as a function of SRH lifetime when $\tau_{SRH} = 0.1$ ns. The inset exhibits the nonradiative recombination effects on the QD laser's α_H factor.

frequencies, all the carrier density variations remain almost constant, whereas beyond the relaxation frequency, typically beyond 2–3 GHz, such variations, especially in the GS an ES levels, are much more pronounced, hence reducing the α_H factor. In order to evaluate the influence of the SRH lifetime, we take the maximum value of the α_H factor at low frequency. The inset of Fig. 3 clearly demonstrates that a smaller nonradiative recombination rate slightly reduces the α_H factor. In recent experimentation, an ultralow α_H factor below unity was measured [5], which unlocks the high potential for chirp-free silicon-based PICs.

B. Impact on the modulation dynamics

Through the small-signal analysis in the previous section, it is easy to extract the modulation transfer function for the QD laser as in [16] if we temporarily leave out the phase equation in Eqs. (12):

$$H(\omega) = \frac{R_0}{\Delta} = \frac{R_0}{R_0 + j\omega R_1 - \omega^2 R_2 - j\omega^3 R_3 + \omega^4}, \quad (14)$$

where Δ is the determinant of the matrix in Eqs. (12) and four parameters which characterize $H(\omega)$ are defined by

$$R_0 = \omega_R^2 \omega_{R0}^2 - \gamma_{23}\gamma_{44}(\gamma_{11}\gamma_{32} + \gamma_{12}\gamma_{31}),$$

$$R_1 = \omega_R^2 \Gamma_0 + \omega_{R0}^2 \Gamma - \gamma_{23}\gamma_{32}(\gamma_{11} + \gamma_{44}) - \gamma_{12}\gamma_{23}\gamma_{31},$$

$$R_2 = \omega_R^2 + \Gamma_0 \Gamma + \omega_{R0}^2 - \gamma_{23}\gamma_{32},$$

$$R_3 = \Gamma_0 + \Gamma,$$

where the relaxation resonance frequency ω_R and damping factor Γ are approximately defined as

$$\omega_R^2 = \gamma_{33}\gamma_{44} - \gamma_{34}\gamma_{43}, \quad \Gamma = \gamma_{33} + \gamma_{44}$$

and, with the same method, the two other parameters are

$$\omega_{R0}^2 = \gamma_{11}\gamma_{22} - \gamma_{12}\gamma_{21}, \quad \Gamma_0 = \gamma_{11} + \gamma_{22}.$$

By utilizing the already defined set of γ, the damping factor Γ can be rewritten as follows:

$$\Gamma = \Gamma_p v_g a_{GS} S_{GS} + \frac{1}{2N_B}\frac{N_{ES}}{\tau_{GS}^{ES}} + \frac{1 - \rho_{ES}}{\tau_{ES}^{GS}}$$
$$+ \frac{1}{\tau_{GS}^{\mathrm{spon}}} + \frac{\Gamma_p \beta_{sp} N_{GS}}{\tau_{GS}^{\mathrm{spon}} S_{GS}} + \frac{2}{\tau_{SRH}}, \quad (15)$$

where the steady-state relationship $1/\tau_p - \Gamma_p v_g g_{GS} = \Gamma_p \beta_{sp} N_{GS}/(\tau_{GS}^{\mathrm{spon}} S_{GS})$ has been used. It is important to stress that Eq. (15) gives the explicit dependence of the damping factor of the QD laser on the SRH lifetime.

The modulation dynamics of the QD laser is depicted in Fig. 4. It shows that the smaller nonradiative recombination suppresses the resonance peak because the nonradiative recombination shortens the total carrier lifetime. Consequently, as shown in Fig. 5, the damping factor is enhanced [see also Eq. (15)], and the 3-dB bandwidth shrinks. This result is consistent with a recent numerical article about the QD laser model in which the turn-on delay dynamics was simulated by varying the timescale ratio between carrier and photon lifetimes [17]. In our hypothesis, varying the SRH recombination time will definitely change that ratio and then influence the damping of the solitary laser. As described hereinafter, we
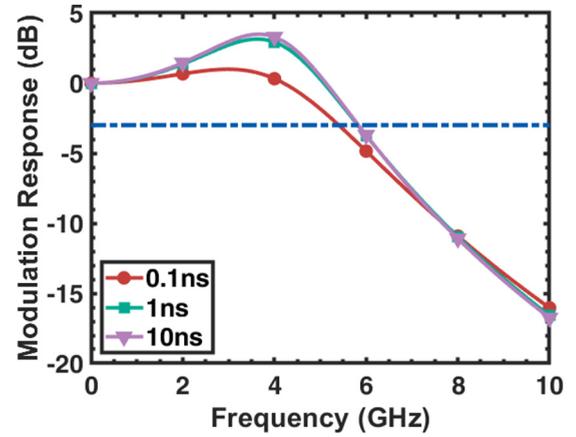

FIG. 4. Nonradiative recombination effects on the QD laser's modulation dynamics. The blue dashed line signifies the position of 3-dB modulation response power.

also find that the higher this damping is, the more resistant the laser is to optical feedback.

IV. EFFECT OF SHOCKLEY-READ-HALL RECOMBINATION ON THE REFLECTION SENSITIVITY

In this section, the laser's feedback sensitivity is analyzed through the numerical simulations, including bifurcation diagrams, time series, and phase portraits. In particular, the evolution of the first Hopf bifurcation is investigated in detail along with the different chaotic bubbles. Both short- and long-delay regimes are considered. The difference between these two regimes is largely driven by the ratio between the relaxation oscillation frequency υ_{RO} and the external cavity mode frequency υ_{ext} [18]. Thus, when $\upsilon_{RO} < \upsilon_{\mathrm{ext}}$, the laser operates within the short-delay regime. On the contrary, when $\upsilon_{RO} > \upsilon_{\mathrm{ext}}$, the long-delay regime is preferred, as shown below. Our QD laser rate equation, that is, Eqs. (1), (2), (3), (9), and (10), can be solved by using the fourth-order Runge-Kutta method. Attention needs to be paid so that, during the simulation process, the time step is 0.5 ps and the time span is 2 μs. For the sake of simplicity, the initial phase is set to be zero, and the pump current is fixed at $2I_{th}$.
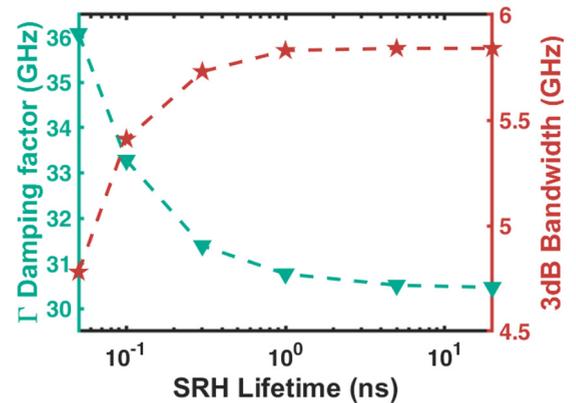

FIG. 5. Nonradiative recombination effects on the QD laser's damping factor and 3-dB bandwidth.
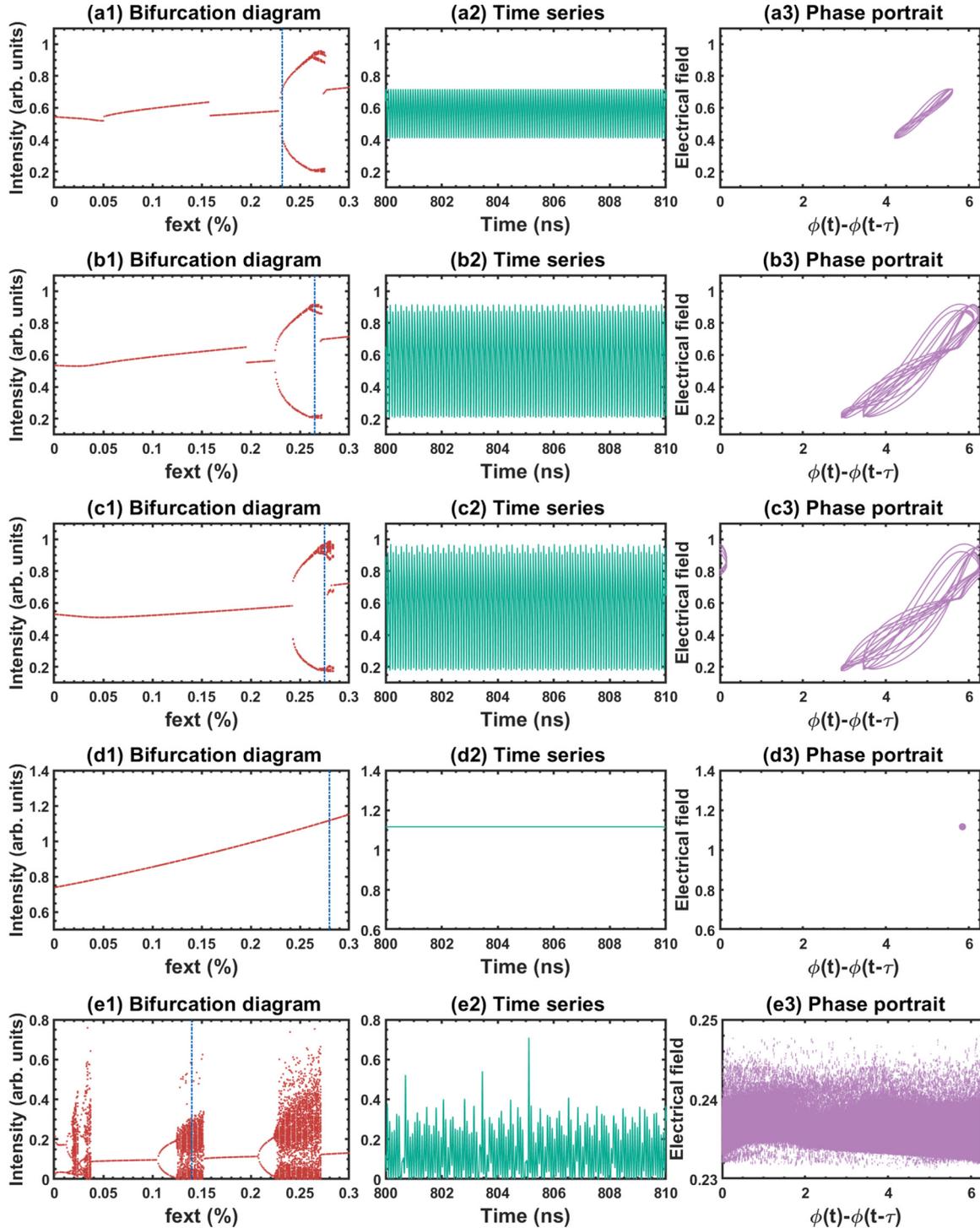
FIG. 6. Numerically computed bifurcation diagrams, time series, and phase portraits in the first, second, and third columns, respectively, for different values of τ_{SRH} in the short-cavity regime ($L = 4$ cm): (a) $\tau_{SRH} = 10$ ns and $f_{est} = 0.232$, (b) $\tau_{SRH} = 5$ ns and $f_{est} = 0.265$, (c) $\tau_{SRH} = 1$ ns and $f_{est} = 0.275$, (d) $\tau_{SRH} = 0.1$ ns and $f_{est} = 0.28$, and (e) the corresponding QW laser and $f_{est} = 0.14$. The blue vertical dashed lines in the first column mark the exact f_{est} value taken in the second and third columns.

A. Short-cavity regime

In PICs, the short-cavity regime is dominant since reflection distances of a few centimeters easily take place due to the presence of many integrated optical components. Obviously, such a situation does have strong consequences on the device

physics. As the relaxation frequency υ_{RO} is smaller than the external cavity frequency υ_{ext}, the number of possible degrees of freedom is substantially reduced, meaning that rich dynamical phenomena can be observed under short delay times such as regular pulse packages [18]. Although some recent studies
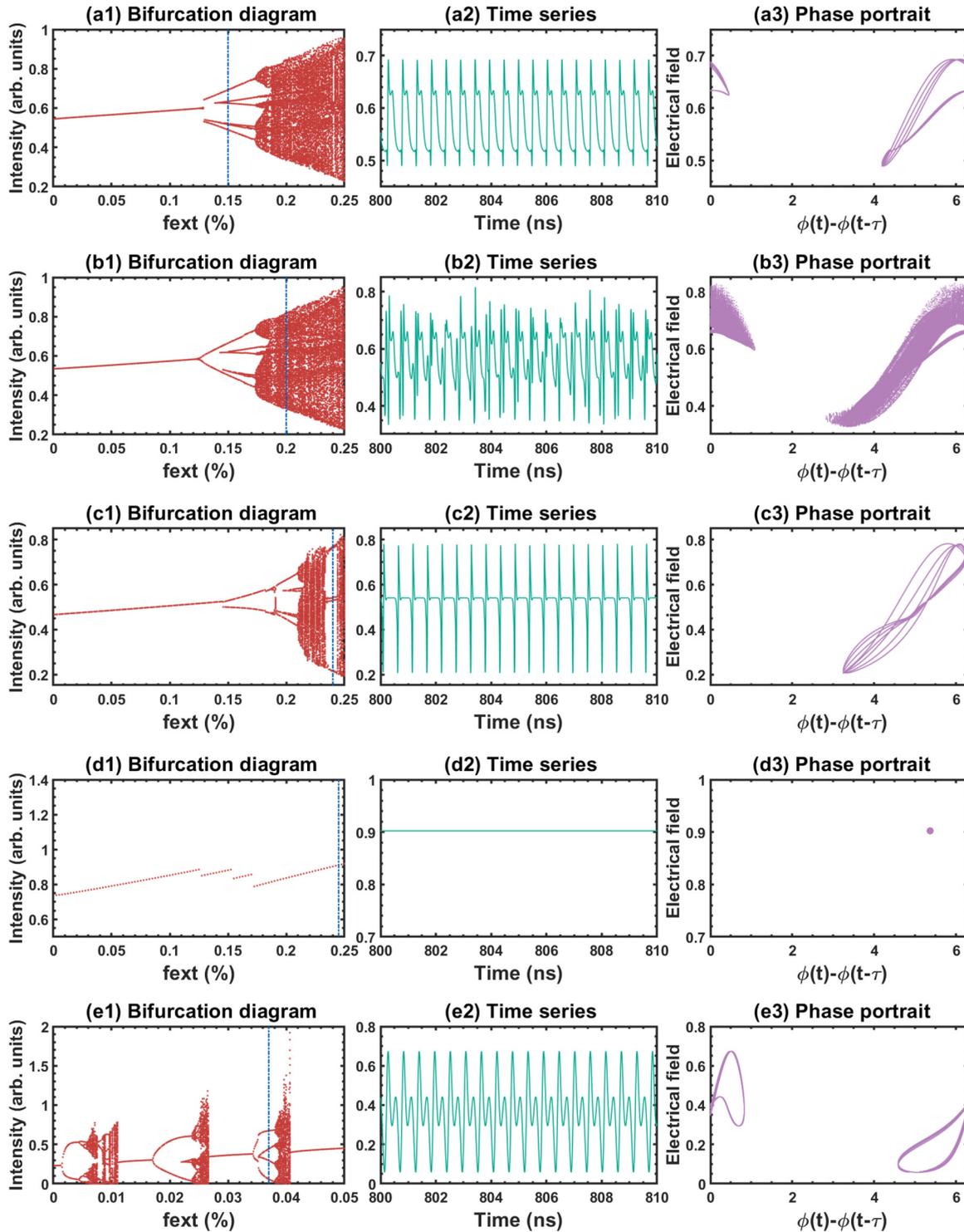
FIG. 7. Numerically computed bifurcation diagrams, time series, and phase portraits in the first, second, and third columns, respectively, for different values of τ_{SRH} in the long-cavity regime (L = 30 cm): (a) τ_{SRH} = 10 ns and f_{est} = 0.15, (b) τ_{SRH} = 5 ns and f_{est} = 0.20, (c) τ_{SRH} = 1 ns and f_{est} = 0.24, (d) τ_{SRH} = 0.1 ns and f_{est} = 0.245, and (e) the corresponding QW laser and f_{est} = 0.037. Blue vertical dashed lines in the first column mark the exact f_{est} value taken in the second and third columns.

have experimentally pioneered the short-cavity regime using silicon photonic devices [19,20], they are usually restricted to very specific operating feedback conditions. Therefore, a thorough numerical investigation is still required in order to reach a complete overview of the laser's dynamical response under various feedback conditions. In a prior work [21], we

presented some initial arguments showing that any decrease of the SRH recombination lifetime yields better laser stability performance, provided the α_H factor is large enough (i.e., $\alpha_H \sim 2$). In this paper, we extend the analysis of the SRH lifetime by considering an α_H-factor value as small as 0.5, which corresponds to recent measured values on epitaxial QD lasers

[5]. Figure 6 displays the bifurcation diagrams, the time series, and the phase portraits extracted from the corpuscular QD laser rate equations with respect to the nonradiative recombination lifetime τ_{SRH}. We assume an external cavity length of $L = 4$ cm. For each value of the feedback strength f_{est}, a normalized output electrical intensity is plotted whenever local maxima and minima occur in the time series. The impact of the SRH lifetime on the bifurcation diagram is unlocked in Fig. 6, showing that any decrease in τ_{SRH} from Figs. 6(a) to 6(d) makes the bifurcation diagram less complex. As one can see, eventually, at $\tau_{SRH} = 0.1$ ns, the periodic region almost disappears, leaving only stable operation.

As mentioned before, it is important to stress that the first Hopf bifurcation is tightly dependent on τ_{SRH}. Thus, in Figs. 6(a)–6(d), when τ_{SRH} decreases from 10 to 0.1 ns, the first Hopf bifurcation turns up at larger values of f_{est}, which means that the stable operation area associated with mode 1 is expanded. In recent experiments, the epitaxial QD laser on silicon demonstrated very good stability in the short-cavity regime with the occurrence of possible periodic oscillations but without chaotic operation, which is in agreement with our simulation results [20]. This inherent property is usually explained as being due to the small α_H factor, the large damping, and the absence of higher-energy states involved in the lasing emission process. Here, we demonstrate that the SRH recombination constitutes an additional mechanism playing a significant role in the evolution of the reflection sensitivity. Lowering τ_{SRH} increases the resistance against optical feedback, which is exactly what happens in epitaxial QD lasers compared to their counterparts grown on native substrate. For comparison, Fig. 6(e1) depicts the corresponding bifurcation diagram of the QW laser. The main parameter different from Fig. 6(a1) is the α_H factor, which is about 2 near threshold [22], whereas in this case, the SRH recombination lifetime is neglected. Here, we retrieve a typical bifurcation scenario with a bifurcation cascade leading to chaos operation with the increase of f_{est} [23].

B. Long-cavity regime

In this section, we analyze the dynamics of epitaxial QD lasers on silicon operating in the long-cavity regime. This regime is also of paramount importance because under some circumstances the external cavity length in PICs may also be longer than expected, leading to a situation where the condition $\upsilon_{RO}/\upsilon_{ext} > 1$ is satisfied. To this end, the number of possible degrees of freedom drastically increases, meaning that the dynamical behaviors can be strongly different from those arising in the short-cavity regime. Figure 7 displays the

bifurcation diagrams, the time series, and the phase portraits extracted from Eqs. (2) and (4) for a fixed value of the external cavity length of $L = 30$ cm and for different values of the nonradiative recombination lifetime τ_{SRH}. As seen from the first column in Figs. 7(a)–7(c), the route to chaos can be observed in the bifurcation diagram, whereas chaotic bubbles vanish, which is also illustrated by the time series in the second column. In addition, we also retrieve the importance of the increase of τ_{SRH} on the first Hopf bifurcation. When this occurs, like in epitaxial QD lasers, it slightly shifts the first Hopf bifurcation point to higher values of f_{est}, here from $f_{est} = 0.1275$ to $f_{est} = 0.146$, which is consistent with the results obtained in the short-cavity regime. Interestingly, in Fig. 7(d), we notice that only stable operation prevails at any time. This situation exactly corresponds to the recent experimental feedback results in epitaxial QD lasers in which no chaotic operation was observed [24]. Finally, the QW laser with a larger α_H factor and negligible SRH recombination leads to a much more complex dynamics. As seen in Fig. 7(e), multiple chaotic bubbles occur, while the period-doubling bifurcation cascade exists until the outbreak of chaos.

V. CONCLUSION

To sum, we have semianalytically and numerically investigated the impact of the SRH recombination on the QD laser's static and dynamical characteristics. Considering the epitaxial defects induced by threading dislocations, we showed that through the small-signal analysis the α_H factor is reduced by decreasing the τ_{SRH} values. In relation to the modulation dynamics, a narrower 3-dB bandwidth but larger damping factor are found in QD laser systems with a fast nonradiative recombination lifetime. Indeed, changing the SRH recombination time changes the timescale ratio between the carrier and photon lifetime, which then changes the damping of the turn-on dynamics of the solitary laser. The higher this damping is, the higher the reflection sensitivity is. To this end, we showed that the chaotic region shrinks and the first Hopf bifurcation point is shifted to higher feedback values under different external cavity regimes. Such results therefore show that the SRH recombination lifetime plays a detrimental role not only in the static characteristics but also in the feedback dynamics subject to the optical feedback of QD lasers directly grown on Si. Our work yields insights into the design of feedback-resistant lasers for future PICs operating without an optical isolator. It also motivates further experimental investigations with epitaxial QD lasers having a small α_H factor and subject to optical feedback.

[1] K. Nishi, K. Takemasa, M. Sugawara, and Y. Arakawa, IEEE J. Sel. Top. Quantum Electron. **23**, 1 (2017).

[2] J. C. Norman, D. Jung, Z. Zhang, Y. Wan, S. Liu, C. Shang, R. W. Herrick, W. W. Chow, A. C. Gossard, and J. E. Bowers, IEEE J. Quantum Electron. **55**, 1 (2019).

[3] D. Liang and J. E. Bowers, Nat. Photon. **4**, 511 (2010).

[4] F. Grillot, J. C. Norman, J. Duan, Z. Zhang, B. Dong, H. Huang, W. W. Chow, and J. E. Bowers, Nanophotonics **9**, 1271 (2020).

[5] J. Duan, H. Huang, D. Jung, Z. Zhang, J. Norman, J. Bowers, and F. Grillot, Appl. Phys. Lett. **112**, 251111 (2018).

[6] D. Inoue, D. Jung, J. Norman, Y. Wan, N. Nishiyama, S. Arai, A. C. Gossard, and J. E. Bowers, Opt. Express **26**, 7022 (2018).

[7] H. Huang, L.-C. Lin, C.-Y. Chen, D. Arsenijević, D. Bimberg, F.-Y. Lin, and F. Grillot, Opt. Express **26**, 1743 (2018).

[8] J. Norman, Ph.D. thesis, University of California, Santa Barbara, 2018.

[9] K. Veselinov, F. Grillot, C. Cornet, J. Even, A. Bekiarski, M. Gioannini, and S. Loualiche, IEEE J. Quantum Electron. **43**, 810 (2007).

[10] R. Lang and K. Kobayashi, IEEE J. Quantum Electron. **16**, 347 (1980).

[11] V. Rottschäfer and B. Krauskopf, Int. J. Bifurcation Chaos **17**, 1575 (2007).

[12] M. C. Soriano, J. García-Ojalvo, C. R. Mirasso, and I. Fischer, Rev. Mod. Phys. **85**, 421 (2013).

[13] T. Erneux and P. Glorieux, *Laser Dynamics* (Cambridge University Press, Cambridge, 2010).

[14] M. Saldutti, A. Tibaldi, F. Cappelluti, and M. Gioannini, Photon. Res. **8**, 1388 (2020).

[15] S. Chen, W. Li, J. Wu, Q. Jiang, M. Tang, S. Shutts, S. N. Elliott, A. Sobiesierski, A. J. Seeds, I. Ross, P. M. Smowton, and H. Liu, Nat. Photon. **10**, 307 (2016).

[16] C. Wang, F. Grillot, and J. Even, IEEE J. Quantum Electron. **48**, 1144 (2012).

[17] B. Globisch, C. Otto, E. Schöll, and K. Lüdge, Phys. Rev. E **86**, 046201 (2012).

[18] T. Heil, I. Fischer, W. Elsäßer, and A. Gavrielides, Phys. Rev. Lett. **87**, 243901 (2001).

[19] A. Karsaklian Dal Bosco, K. Kanno, A. Uchida, M. Sciamanna, T. Harayama, and K. Yoshimura, Phys. Rev. E **92**, 062905 (2015).

[20] B. Dong, J.-D. Chen, F.-Y. Lin, J. C. Norman, J. E. Bowers, and F. Grillot, Phys. Rev. A **103**, 033509 (2021).

[21] S. Zhao, J. Duan, B. Dong, and F. Grillot, Proc. SPIE **11680**, 62 (2021).

[22] B. Riou, N. Trenado, F. Grillot, F. Mallecot, V. Colson, M. Martineau, B. Thédrez, L. Silvestre, D. Meichenin, K. Merghem, and A. Ramdane, in *Proceedings of IEEE European Conference on Optical Communication (ECOC)* (IEEE, Piscataway, NJ, 2003), p. 85.

[23] A. Hohl and A. Gavrielides, Phys. Rev. Lett. **82**, 1148 (1999).

[24] J. Duan, H. Huang, B. Dong, D. Jung, J. C. Norman, J. E. Bowers, and F. Grillot, IEEE Photon. Technol. Lett. **31**, 345 (2019).